First-principles bulk-layer model for dielectric and piezoelectric responses in superlattices

J. Bonini, J. W. Bennett, P. Chandra, and K. M. Rabe

First-Principles Bulk-Layer Model for Dielectric and Piezoelectric Responses in Superlattices

J. Bonini, J. W. Bennett, P. Chandra, and K. M. Rabe

Department of Physics and Astronomy
Rutgers University, Piscataway, NJ 08854

In the first-principles bulk-layer model the superlattice structure and polarization are determined by first-principles computation of the bulk responses of the constituents to the electrical and mechanical boundary conditions in an insulating superlattice. In this work the model is extended to predict functional properties, specifically dielectric permittivity and piezoelectric response. A detailed comparison between the bulk-layer model and full first-principles calculations for three sets of perovskite oxide superlattices, $PbTiO_3/BaTiO_3$, $BaTiO_3/SrTiO_3$ and $PbTiO_3/SrTiO_3$, is presented. The bulk-layer model is shown to give an excellent first approximation to these important functional properties, and to allow for the identification and investigation of additional physics, including interface reconstruction and finite size effects. Technical issues in the generation of the necessary data for constituent compounds are addressed. These results form the foundation for a powerful data-driven method to facilitate discovery and design of superlattice systems with enhanced and tunable polarization, dielectric permittivity, and piezoelectric response.

INTRODUCTION

Ongoing progress in atomic scale precision growth of perovskite oxide superlattices enables exploration of an ever increasing variety of systems.[1–4] There is particular interest in systems in which the layering gives rise to distinctive functional properties, including enhancement of properties such as the piezoelectric response over those of either constituent [5]. While the microscopic origins of such behavior could include symmetry breaking by artificial structuring, a high density of atomically and electronically reconstructed interfaces, and finite size effects in the unit-cell-scale constituent layers, early experimental and first-principles investigation of $BaTiO_3/SrTiO_3$ superlattices suggested that the properties of superlattices, even with ultrashort periods, can in fact be largely predicted by a "bulk-layer" model in which the properties of the superlattice are obtained by considering the bulk response to the changes in mechanical and electrical boundary conditions imposed on each constituent layer by lattice matching and approximate polarization matching [6–9].

For a given constituent material, the bulk response to the changes in mechanical boundary conditions corresponding to lattice matching is readily computed in a first-principles framework via a strained-bulk calculation in which two lattice vectors of the bulk material are fixed to match the substrate at the interface plane, and other structural parameters are relaxed [10, 11]. The development of first-principles methods allowing the calculation of structure and properties in nonzero uniform electric fields [12] and the subsequent recognition of the displacement field $\mathbf{D}$ as the fundamental electrostatic variable [13] allow a quantitative determination of how a constituent layer responds to changes in electrical boundary conditions, including a correct description of nonlinear behavior at high fields. The use of these nonlinear

first-principles electric-elastic constitutive relations enables the model to capture behavior beyond a simple averaging of end point properties.

The bulk-layer model has been successfully applied to a number of perovskite superlattice systems. For $BaTiO_3/SrTiO_3$, it accounts for the observed polarization of the $SrTiO_3$ layers [6, 7] and the evolution of the structure and polarization with epitaxial strain [14–16]. Extension to the case of perovskite superlattices with "charge-mismatched" constituents (for example, $A^{3+}B^{3+}O_3/A'^{2+}B'^{4+}O_3$) [17] yielded quantitative predictions for the epitaxial strain dependence of the structure and polarization of $PbTiO_3/BiFeO_3$ superlattices [17, 18]. A version of the model was also used to study the response of ferroelectric capacitors with metallic electrodes [19]. For a broader range of superlattice systems, the predictions of the bulk-layer model can be expected to provide a good starting point from which interface and finite size effects can be identified and analyzed as contributions from such effects are absent in the model.

In this manuscript, we show how to extend this definitive implementation of the bulk-layer model to the prediction of dielectric and piezoelectric responses in insulating superlattices. For three prototypical titanate superlattice systems, $PbTiO_3/BaTiO_3$, $BaTiO_3/SrTiO_3$, and $PbTiO_3/SrTiO_3$, we generate the necessary information about the bulk constituent compounds, apply the bulk-layer model to the prediction of superlattice structure, polarization, dielectric and piezoelectric responses and show that the model can capture the essential trends with composition by comparing to results using first-principles methods of the full superlattices. Thus, using only a database of computed bulk constituent electric-elastic constitutive relations, it should be possible to map out a large configuration space of superlattice combinations and investigate the microscopic origins of their

functional properties, leading to a powerful data-driven method to facilitate discovery and design of superlattice systems with enhanced and tunable polarization, dielectric permittivity and piezoelectric response.

METHODS

Bulk-Layer Model

The constituent layers of the superlattice are modeled as strained-bulk materials [10, 11] responding uniformly to the changes in mechanical and electrical boundary conditions produced by the superlattice, specifically lattice matching and absence of free charge at the interface. Here, we consider superlattices epitaxially coherent with a chosen substrate (here, (001) $SrTiO_3$), so that the lattice matching is implemented by fixing two lattice vectors (here, $\mathbf{a} = (a_0, 0, 0)$ and $\mathbf{b} = (0, a_0, 0)$) to match the substrate at the interface plane. The absence of free charge corresponds to the condition that the displacement field $\mathbf{D}$ be uniform throughout the system [13]. Throughout this work we specialize to tetragonal systems where $\mathbf{D}$, $\mathbf{E}$, and $\mathbf{P}$ are along the four-fold axis with magnitudes given by D, E, and P. The case of charge-mismatched constituents can be treated by including fixed interface charges σ as in [17]. For the specified fixed lattice vectors, each constituent material α is described by the electric-elastic constitutive relations $U(D; \alpha)$, $c(D; \alpha)$, $E(D; \alpha)$, and $P(D; \alpha)$ corresponding to the energy per unit cell (taken relative to its minimum value), out-of-plane lattice parameter, electric field, and polarization, respectively. We note that $E(D)$ is related to $U(D)$ through $E(D) = \frac{1}{\Omega(D)} \frac{dU}{dD}$ [13], where Ω is the unit cell volume. For the superlattice consisting of periodic repeats of k layers of unit cell thickness n_i; $i = 1, ...k$, with superlattice period $N = \sum_i n_i$, the total energy is taken as the sum of the energies of the individual layers:

$$U(D) = \sum_i x_i U(D - \sigma_i; \alpha_i) \quad (1)$$

where $x_i = n_i/N$ and $\sigma_i = \sum_{j=1}^{i-1} \sigma_{j,j+1}$, where $\sigma_{j,j+1}$ is the fixed interface charge at the interface between layer j and layer $j + 1$, and $\sigma_1 = 0$.

We consider situations in which the voltage drop V across the sample is controlled, with the $V = 0$ short-circuit boundary condition corresponding to the periodic boundary conditions used in first-principles calculations. In practice, we first construct

$$V(D) = \sum_i n_i E(D - \sigma_i; \alpha_i) c(D - \sigma_i; \alpha_i) \quad (2)$$

The D that corresponds to the target V is obtained by solving $V(D) = V$ and if there are multiple solutions, then choosing the one that gives the lowest value

of $U(D)$. For $V = 0$, this is equivalent to minimizing $U(D)$ with respect to D as in [17]. When the model is solved at $V = 0$, the D which solves the model is precisely the zero field polarization (P) of the superlattice system. This follows from the definition $D = P + \epsilon_0 E$: with zero overall voltage the total external field is also zero and $D = P$. We then construct $c_{tot}(D) = \sum_i n_i c(D - \sigma_i; \alpha_i)$, $E_{ext}(D) = V(D)/c_{tot}(D)$, and the derivatives of each with respect to D, from which we obtain the zero-stress relative permittivity or dielectric constant $\kappa_{33} = \epsilon_{33}/\epsilon_0 = \frac{1}{\epsilon_0}(dE_{ext}/dD)^{-1}$ and the piezoelectric response $d_{33} = c_{tot}^{-1}(dc_{tot}/dD)(dE_{ext}/dD)^{-1} = g_{33}\epsilon_{33}$ where $g_{33} = c_{tot}^{-1} dc_{tot}/dD$. Note that the dielectric and piezoelectric constants used in this work are for fixed in-plane lattice constants (see supplemental material [20]).

The systems examined in this manuscript are two-component superlattices with fixed interface charge equal to zero. In this case equations (1) and (2) reduce to:

$$U(D) = xU(D; \alpha_1) + (1 - x)U(D - \sigma_{int}; \alpha_2) \quad (3)$$

$$V(D) = Nxc(D; \alpha_1)E(D; \alpha_1) \\ + N(1 - x)c(D - \sigma_{int}; \alpha_2)E(D - \sigma_{int}; \alpha_2) \quad (4)$$

where we include σ_{int} for validity for charge-mismatched constituents; in the charge-matched systems considered here, $\sigma_{int} = 0$. As discussed above, the D that corresponds to the target V is obtained by solving $V(D) = V$ and if there are multiple solutions, choosing the one that gives the lowest value of $U(D)$. From this, polarization, out-of-plane lattice constants, and dielectric and piezoelectric responses can be immediately obtained.

First Principles Calculations

We performed first-principles density-functional-theory calculations with the local density approximation (LDA) using the ABINIT package [21–23]. Norm-conserving pseudopotentials were generated with the Opium code [24, 25]. An energy cutoff of 800 eV was used with a $10 \times 10 \times 10$ Monkhorst-Pack grid to sample the Brillouin zone for 5-atom-unit-cell systems, and equivalent k point densities for the superlattice systems [26]. Structural relaxations were performed with a force threshold of 10 meV/Å, except for $SrTiO_3$ fixed displacement field calculations where the slightly polar structure required a stricter convergence of 1 meV/Å. In plane lattice constants are fixed to that of $SrTiO_3$, here 3.857 Å. For the superlattices, polarization was computed using the Berry phase formalism [27], and dielectric and piezoelectric responses were computed using density functional perturbation theory (DFPT) [28–30]. The electric constitutive relations for the materials $BaTiO_3$, $PbTiO_3$ and $SrTiO_3$ were computed using fixed displacement field calculations for the five

atom unit cell [13]. Convergence issues encountered (and the measures taken to remedy them) in performing the fixed displacement-field calculations are discussed in the supplemental material [20].

RESULTS

Electric-Elastic Constituitive Relations

Figure 1 shows the electric-elastic constitutive relations for $SrTiO_3$, $BaTiO_3$, and $PbTiO_3$ computed for displacement fields ranging from $D = 0$ to just above the ground state polarization of $PbTiO_3$ ($D = 0.85$ C/m^2). The ferroelectrics $BaTiO_3$ and $PbTiO_3$ display a characteristic double well in the energy and a non-monotonic behavior of the electric field with displacement field, consistent with the results for $PbTiO_3$ shown in [31]. $SrTiO_3$ displays its characteristically flat energy well and nonlinear evolution of electric field with displacement field [32], which, as we will discuss below, gives rise to very large dielectric and piezoelectric responses for superlattices with large $SrTiO_3$ fraction. Within our first-principles framework, $SrTiO_3$ is very slightly polar, with a shallow double well and non-monotonic electric field at small D as shown in the insets of Figure 1; the experimental observation that $SrTiO_3$ is paraelectric down to low temperatures is attributed to the effects of quantum fluctuations [33]. In the bottom panel of Figure 1 the derivative of each $E(D; \alpha)$ curve with respect to D is shown. At large D values this derivative begins to decrease in $BaTiO_3$, indicating an anomalous softening discussed below. The bulk structural parameters, polarization, dielectric permittivity, and piezoelectric response are tabulated in the supplemental material [20].

Superlattice Properties

Fig. 2a shows the polarization for $PbTiO_3/BaTiO_3$ superlattices as a function of x, the layer fraction of $BaTiO_3$. The bulk-layer model shows a bowing below the linear interpolation between pure $BaTiO_3$ and pure $PbTiO_3$. The first-principles results show only a very weak dependence on the superlattice period, converging quite rapidly to the model curve with increasing superlattice period for a given x. The x dependence of model tetragonality c/a, where $c = c_{tot}/N$ shown in Fig. 2a is so strongly bowed that it is nonmonotonic. Here too, the first-principles results do not show a strong dependence on the superlattice period and converge quite rapidly to the model curve with increasing superlattice period for a given x. The bulk-layer model response functions ϵ_{33} and d_{33} also show distinctly nonlinear behavior, with a change in curvature at an intermediate value of x as well as non-monotonic behavior for ϵ_{33}. The first-principles
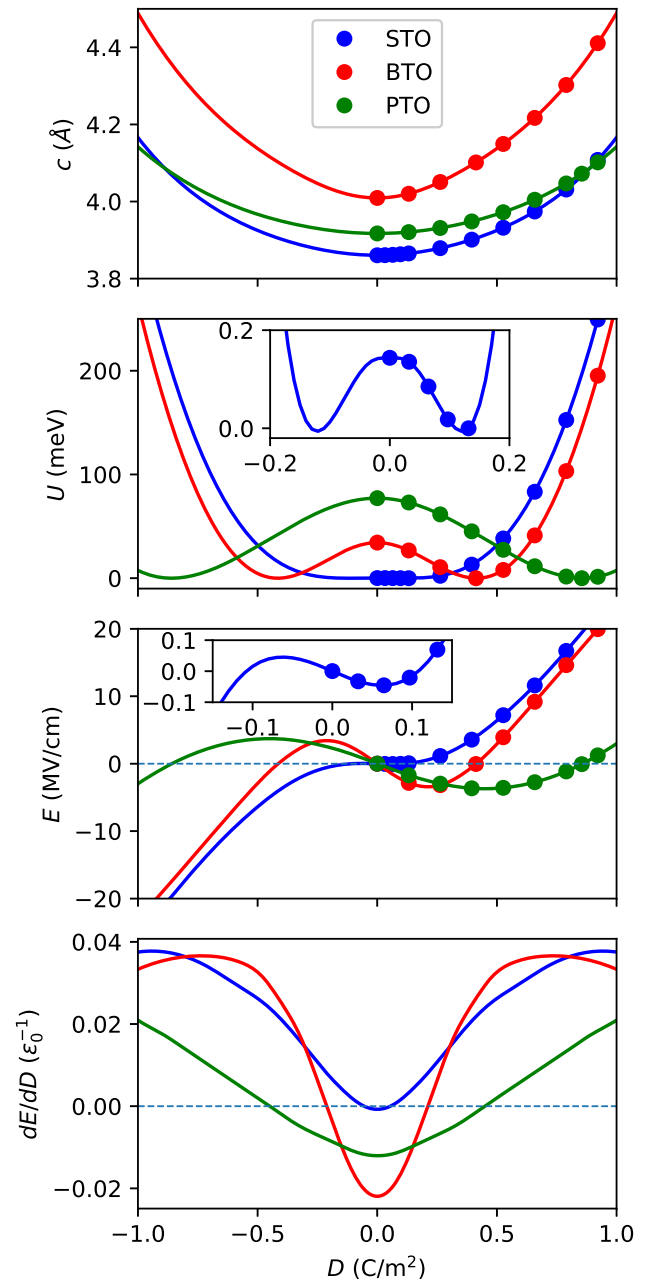

FIG. 1: Computed electric-elastic constitutive relations for $SrTiO_3$, $BaTiO_3$, and $PbTiO_3$. Filled circles show the calculated values and the solid curves are spline fits. The definite parity of each function is used to obtain the results for negative D. The insets zoom in on the slight polar instability computed for $SrTiO_3$. The bottom figure shows the derivatives of the spline fits shown in the E plot with respect to D.

results for the response functions show a stronger dependence on the superlattice period, with substantial en-

hancement over the model and with the shortest-period (small N), PbTiO$_3$-richest (small x) superlattices displaying enhancement even above the values of each pure constituent. With increasing period, these values converge quite accurately to the model. This is illustrated by the insets, which show that linear extrapolation of the computed responses for $n:n$ superlattices versus $1-1/N$ to $N = \infty$ matches the computed model value. This is as expected, since the interface and finite size effects in individual superlattices should become negligible in this limit, and the physics will be dominated by the effects included in the bulk-layer model, which depends only on x and is independent of the total superlattice period.

The results for the BaTiO$_3$/SrTiO$_3$ superlattices, shown in Fig. 2b, show an upward bowing for the polarization (opposite to that of PbTiO$_3$/BaTiO$_3$), and near linearity for the tetragonality as a function of x, the layer fraction of SrTiO$_3$. The first principles results show weak dependence on the superlattice period. The near-flatness of the energy well $U(D;\text{STO})$, shown in the main part of Fig 1c, leads to the large dielectric and piezoelectric responses in the SrTiO$_3$-rich (large x) superlattices. As discussed below this same feature of $U(D;\text{STO})$ also leads to certain deviations from the model curves at large SrTiO$_3$ volume fraction, including the polarization, and dielectric and piezoelectric responses of SrTiO$_3$-rich (large x) superlattices.

Finally, the results for the PbTiO$_3$/SrTiO$_3$ superlattices, shown in Fig. 2c, show only slight bowing for the polarization and the tetragonality as a function of x, the layer fraction of SrTiO$_3$. The first-principles results show negligible dependence on superlattice period, lying on or very close to the model curves even for the shortest-period superlattices. The dielectric response grows even more rapidly with x than for BaTiO$_3$/SrTiO$_3$ (note the difference in the vertical scale). The piezoelectric response, in contrast, shows a striking suppression below the pure constituent values at intermediate values of x, which is also clearly evident in the first-principles results.

DISCUSSION

Analysis of Model Results

The bowing in the x dependence of the polarization for all three systems can be understood by considering $x = 0.5$. There, the minimization of $U(D)$ with respect to D requires $dU(D;\alpha_1)/dD = -dU(D;\alpha_2)/dD$, and examination of Fig. 1 immediately shows that the value of D, and thus of P, that minimizes $U(D)$ is between the values that minimize the individual $U(D;\alpha_i)$. For the superlattice systems containing BaTiO$_3$, the relatively high stiffness of BaTiO$_3$ around its minimum gives minimal values of D for $U(D)$ that are closer to that of BaTiO$_3$ (lower than the average D for PbTiO$_3$/BaTiO$_3$

and higher than the average D for BaTiO$_3$/SrTiO$_3$), corresponding to the observed bowings. The low stiffness of PbTiO$_3$ combines with the flatness of SrTiO$_3$ to give a minimizing D close to and just slightly below the average, corresponding to the small downward bowing for PbTiO$_3$/SrTiO$_3$.

The deviations from the simple linear interpolation values in the tetragonality (c/a) can be similarly understood by considering $x = 0.5$. In PbTiO$_3$/BaTiO$_3$, the value of c computed at the average D of the two constituents $(\bar{D})$, that is $0.5(c(\bar{D};\text{PbTiO}_3) + c(\bar{D};\text{BaTiO}_3))$ is 4.102 Å, above the linear interpolation value of 4.087 Å. The downward bowing in P, so that the D at $x = 0.5$ is well below $\bar{D}$, is thus completely responsible for lowering the value of c/a at $x = 0.5$ so far as to lead to the nonmonotonic dependence on x. In contrast, for BaTiO$_3$/SrTiO$_3$ the upward shift of c/a computed at $\bar{D}$ relative to the linear interpolation value is almost equal and opposite in sign to the downward shift due to the smaller bowing of P, so that c/a vs x is almost linear. Finally, for PbTiO$_3$/SrTiO$_3$, the two shifts are comparable in magnitude and both downward, accounting for the observed downward bowing of P.

The dielectric permittivity of the superlattice $\epsilon_{33} = dD/dE_{\text{ext}}$ can equivalently be written in a form where it is expressed in terms of the behavior of individual layers as:

$$\epsilon_{33} = \frac{\sum_i x_i c(D;\alpha_i)}{\sum_i x_i c(D;\alpha_i)\frac{dE(D;\alpha_i)}{dD}} \qquad (5)$$

The non-monotonic behavior of ϵ_{33} in PbTiO$_3$/BaTiO$_3$, can be partly attributed to an anomaly in the high-D behavior of BaTiO$_3$, with a nonlinear softening for $D > 0.6$ C/m^2, as can be seen in the (red) BaTiO$_3$ dE/dD curve in Figure 1. This arises from proximity in the energy landscape to a highly-polar supertetragonal phase of BaTiO$_3$ which has been predicted to be stable at large negative pressure [34, 35]. While the supertetragonal phase is not even metastable under the mechanical and electrical boundary conditions explored, the values of D achieved in the BaTiO$_3$ layer in superlattices with a large fraction of PbTiO$_3$ are in this anomalous regime. Similarly large values of D are achieved in SrTiO$_3$ layers for PbTiO$_3$/SrTiO$_3$ superlattices with low SrTiO$_3$ fraction. However, as can be seen in the (blue) SrTiO$_3$ dE/dD curve in Figure 1 while dE/dD does begin to soften in SrTiO$_3$ it never decreases in the relevant range of D. Furthermore, the large permittivity of SrTiO$_3$ means that the straightforward effect of more of the system being composed of the high permittivity constituent dominates the evolution of ϵ_{33} with x, and any enhancement due to effects on the energy landscape from a supertetragonal phase are comparably negligible. The dielectric susceptibility of PbTiO$_3$/SrTiO$_3$ is seen to increase more rapidly than in BaTiO$_3$/SrTiO$_3$ (notice the difference in scales between the two plots). While there is

a contribution from the slight softening of SrTiO$_3$ at high D, PbTiO$_3$/SrTiO$_3$ is also the only one of the three systems examined here where one of the constituents has a negative $dE(D;\alpha)/dD$ for a large range of x (see PbTiO$_3$ in Figure 1b at $D < 0.55$). A negative $dE(D;\alpha_i)/dD$ in the denominator of equation (5) increases the susceptibility of the superlattice [36].

The behavior of d_{33} for each system can be understood by first recalling that $d_{33} = \epsilon_{33}g_{33}$. As can be seen in Figure S1 in the supplemental material [20], each system's $g_{33}(x)$ has a bowing following that of the polarization bowing for reasons analogous to those discussed regarding the tetragonality. In PbTiO$_3$/BaTiO$_3$ the downward bowing of $g_{33}(x)$ is so strong that it is nonmonotonic. When multiplied by $\epsilon_{33}(x)$, which has the previously discussed enhancement, the resulting $d_{33}(x)$ is monotonically decreasing, with a change in curvature. For both PbTiO$_3$/SrTiO$_3$ and BaTiO$_3$/SrTiO$_3$ g_{33} is a monotonically decreasing function of x, while ϵ_{33} is monotonically increasing, but their d_{33} curves exhibit qualitatively different behavior. This can be understood by considering how the slope at any given x relates to the slope and magnitudes of ϵ_{33} and g_{33}:

$$\frac{dd_{33}}{dx} = \frac{d\epsilon_{33}}{dx}g_{33}(x) + \epsilon(x)\frac{dg_{33}}{dx}$$

For both BaTiO$_3$/SrTiO$_3$ and PbTiO$_3$/SrTiO$_3$ the first term is always positive and the second term is always negative. Then d_{33} will have a negative slope in regions where the following is satisfied:

$$\frac{1}{g_{33}}|\frac{dg_{33}}{dx}|\epsilon_{33} > \frac{d\epsilon_{33}}{dx}$$

For both SrTiO$_3$ systems $d\epsilon_{33}/dx_{STO}$ comes to dominate in the large x_{STO} limit resulting in a positive slope at large x. If at $x = 0$ the above condition is satisfied, the slope is initially negative and the resulting curve is nonmonotonic, while if the slope is positive the curve can monotonically increase (as in BaTiO$_3$/SrTiO$_3$). In PbTiO$_3$/SrTiO$_3$ the larger ϵ_{33} of PbTiO$_3$ (discussed above), combined with the positive curvature of g_{33} for PbTiO$_3$/SrTiO$_3$, results in the above inequality being satisfied for $x = 0$, leading to the nonmonotonic behavior observed in d_{33} in Figure 2c.

Comparison With First Principles Results

An implicit assumption of the bulk-layer model is that the structure within each constituent layer is uniform. In the full first-principles calculations, the structure within each constituent layer is free to vary, and in particular, the region near the interface can be different from the layer interior. These additional degrees of freedom, together with interface effects, contribute to the larger

responses seen in the full first-principles calculations. This is particularly pronounced in BaTiO$_3$/SrTiO$_3$ and PbTiO$_3$/SrTiO$_3$ superlattices with high SrTiO$_3$ fraction, for which examination of the structure in the SrTiO$_3$ layer shows comparatively large variation within the layer, partly accounting for the discrepancies between the full first-principles superlattice values and the model for ϵ_{33} and d_{33}.

In the results presented here, we have considered 5-atom $P4mm$ structures for the constituent compounds and $1 \times 1 \times N$ $P4mm$ structures for the superlattices, allowing consistent comparisons between the bulk-layer model predictions and the first-principles calculations. In fact, both experimental and theoretical investigations of PbTiO$_3$/SrTiO$_3$ superlattices show that oxygen octahedron rotations appear in the lowest-energy phases [37–39]. For comparison to PbTiO$_3$/SrTiO$_3$ experiments, this model therefore can straightforwardly be extended, as done for the polarization and structure ofPbTiO$_3$/BiFeO$_3$ in [17], by laterally enlarging the unit cells to allow rotations when computing the constitutive relations. The construction of a large database of more complete electric-elastic constituitive relations for a variety of constituents and subsequent search for desirable properties and interesting physics will be the subject of future work. More generally, in superlattice systems where the favored tilt pattern changes across the interface, there will be steric constraints arising from the shared oxygens, tending to propagate oxygen tilt patterns across the interface [40]. This interface effect, not included in the bulk-layer model, will be largest for superlattices with the thinnest constituent layers and become negligible in the limit that the layer thickness will become large.

In PbTiO$_3$/BaTiO$_3$, the dielectric permittivity and piezoelectric responses show strong period-dependent enhancements relative to the bulk-layer model, with the largest enhancements for the shortest period superlattices: 38% in ϵ_{33} for the 1:1 superlattice and 32% in d_{33} for the 2:1 superlattice. For both ϵ_{33} and d_{33}, the highest values at intermediate x are above the values for either constituent. The enhancement over the values predicted by the model signals the contribution of the interfaces, including atomic and electronic reconstruction, and finite size effects. While interfaces and finite size effects appear to significantly enhance these responses the trend captured by the bulk-layer model alone would identify these compositions as a region of interest as ϵ_{33} demonstrated enhancement at the level of the model alone. Detailed comparison with experimental measurements of the system is the subject of paper in preparation.

CONCLUSIONS

In summary, we have extended the first-principles bulk-layer model, which predicts the properties of superlattices from the bulk constituent responses to changing mechanical and electrical boundary conditions, to the prediction of dielectric and piezoelectric responses in insulating superlattices. We have presented a quantitative comparison between the model and full first-principles calculations for three sets of superlattices ($PbTiO_3$/$BaTiO_3$, $BaTiO_3$/$SrTiO_3$ and $PbTiO_3$/$SrTiO_3$) demonstrating that the model provides an excellent first approximation to the polarization, tetragonality, dielectric permittivity and piezoelectric response of these systems allowing the identification of interface and finite-size effect contributions. Expansion of the constituent database will allow the efficient exploration of a large configuration space of superlattices, enabling the data-driven design and discovery of superlattice materials with targeted functional properties.

[1] D. G. Schlom, L.-Q. Chen, C.-B. Eom, K. M. Rabe, S. K. Streiffer, and J.-M. Triscone, Annual Review of Materials Research **37**, 589626 (2007).

[2] J. Junquera and P. Ghosez, Journal of Computational and Theoretical Nanoscience **5**, 20712088 (2008).

[3] M. Dawber and E. Bousquet, MRS Bulletin **38**, 10481055 (2013).

[4] F. Yang, Y. Liang, L.-X. Liu, Q. Zhu, W.-H. Wang, X.-T. Zhu, and J.-D. Guo, Frontiers of Physics **13**, 136802 (2018).

[5] V. R. Cooper and K. M. Rabe, Physical Review B **79**, 180101 (2009).

[6] J. B. Neaton and K. M. Rabe, Applied Physics Letters **82**, 15861588 (2003).

[7] W. Tian, J. C. Jiang, X. Q. Pan, J. H. Haeni, Y. L. Li, L. Q. Chen, D. G. Schlom, J. B. Neaton, K. M. Rabe, and Q. X. Jia, Applied Physics Letters **89**, 092905 (2006).

[8] F. A. Urtiev, V. G. Kukhar, and N. A. Pertsev, Applied Physics Letters **90**, 252910 (2007).

[9] N. A. Pertsev, P.-E. Janolin, J.-M. Kiat, and Y. Uesu, Phys. Rev. B **81**, 144118 (2010).

[10] N. A. Pertsev, A. G. Zembilgotov, and A. K. Tagantsev, Phys. Rev. Lett. **80**, 1988 (1998).

[11] O. Diéguez, K. M. Rabe, and D. Vanderbilt, Phys. Rev. B **72**, 144101 (2005).

[12] I. Souza, J. Íñiguez, and D. Vanderbilt, Phys. Rev. Lett. **89**, 117602 (2002).

[13] M. Stengel, N. A. Spaldin, and D. Vanderbilt, Nature Physics **5**, 304308 (2009).

[14] K. Johnston, X. Huang, J. B. Neaton, and K. M. Rabe, Physical Review B **71**, 100103 (2005).

[15] A. Q. Jiang, J. F. Scott, H. Lu, and Z. Chen, Journal of Applied Physics **93**, 11801185 (2003).

[16] M. Dawber, C. Lichtensteiger, M. Cantoni, M. Veithen, P. Ghosez, K. Johnston, K. M. Rabe, and J.-M. Triscone, Physical Review Letters **95**, 177601 (2005).

[17] C. Cazorla and M. Stengel, Physical Review B **90**, 020101 (2014).

[18] Y. Yang, M. Stengel, W. Ren, X. H. Yan, and L. Bellaiche, Physical Review B **86**, 144114 (2012).

[19] M. Stengel, D. Vanderbilt, and N. A. Spaldin, Physical Review B **80**, 224110 (2009).

[20] See Supplemental Material at [SUPPLEMENT URL] for details on finite displacement field calculations, response values with epitaxial constraints, comparison of the model and linear response values for bulk constituents, tabulated structural information, and results for three component superlattices. This supplement contains references to [12, 13, 21–23, 27, 30, 41–43].

[21] X. Gonze, B. Amadon, P.-M. Anglade, J.-M. Beuken, F. Bottin, P. Boulanger, F. Bruneval, D. Caliste, R. Caracas, M. Ct, T. Deutsch, L. Genovese, P. Ghosez, M. Giantomassi, S. Goedecker, D. Hamann, P. Hermet, F. Jollet, G. Jomard, S. Leroux, M. Mancini, S. Mazevet, M. Oliveira, G. Onida, Y. Pouillon, T. Rangel, G.-M. Rignanese, D. Sangalli, R. Shaltaf, M. Torrent, M. Verstraete, G. Zerah, and J. Zwanziger, Computer Physics Communications **180**, 2582 (2009).

[22] X. Gonze, G. Rignanese, M. Verstraete, J. Betiken, Y. Pouillon, R. Caracas, F. Jollet, M. Torrent, G. Zerah, M. Mikami, P. Ghosez, M. Veithen, J.-Y. Raty, V. Olevano, F. Bruneval, L. Reining, R. Godby, G. Onida, D. Hamann, and D. Allan, Zeitschrift für Kristallographie. **220**, 558 (2005).

[23] X. Gonze, J.-M. Beuken, R. Caracas, F. Detraux, M. Fuchs, G.-M. Rignanese, L. Sindic, M. Verstraete, G. Zerah, F. Jollet, M. Torrent, A. Roy, M. Mikami, P. Ghosez, J.-Y. Raty, and D. Allan, Computational Materials Science **25**, 478 (2002).

[24] J. W. Bennett, Physics Procedia **34**, 1423 (2012).

[25] J. Yang, "Opium - pseudopotential generation project," http://opium.sourceforge.net/ (2018).

[26] H. J. Monkhorst and J. D. Pack, Phys. Rev. B **13**, 5188 (1976).

[27] R. D. King-Smith and D. Vanderbilt, Physical Review B **47**, 1651 (1993).

[28] X. Gonze, Phys. Rev. B **55**, 10337 (1997).

[29] X. Gonze and C. Lee, Phys. Rev. B **55**, 10355 (1997).

[30] X. Wu, D. Vanderbilt, and D. R. Hamann, Physical Review B **72**, 035105 (2005).

[31] J. Hong and D. Vanderbilt, Physical Review B **84**, 115107 (2011).

[32] A. Antons, J. B. Neaton, K. M. Rabe, and D. Vanderbilt, Physical Review B **71**, 024102 (2005).

[33] K. A. Müller and H. Burkard, Phys. Rev. B **19**, 3593 (1979).

[34] O. Diéguez, S. Tinte, A. Antons, C. Bungaro, J. B.

Neaton, K. M. Rabe, and D. Vanderbilt, Phys. Rev. B **69**, 212101 (2004).

[35] S. Tinte, K. M. Rabe, and D. Vanderbilt, Physical Review B **68**, 144105 (2003).

[36] I. Ponomareva, L. Bellaiche, and R. Resta, Phys. Rev. Lett. **99**, 227601 (2007).

[37] E. Bousquet, M. Dawber, N. Stucki, C. Lichtensteiger, P. Hermet, S. Gariglio, J.-M. Triscone, and P. Ghosez, Nature **452**, 732 (2008).

[38] P. Aguado-Puente and J. Junquera, Phys. Rev. B **85**, 184105 (2012).

[39] Y. Zhou and K. M. Rabe, Phys. Rev. B **89**, 214108 (2014).

[40] J. M. Rondinelli and N. A. Spaldin, Phys. Rev. B **82**, 113402 (2010).

[41] N. A. Spaldin, Journal of Solid State Chemistry **195**, 2 (2012).

[42] T. Ikeda, *Fundamentals of piezoelectricity* (Oxford University Press, 1997).

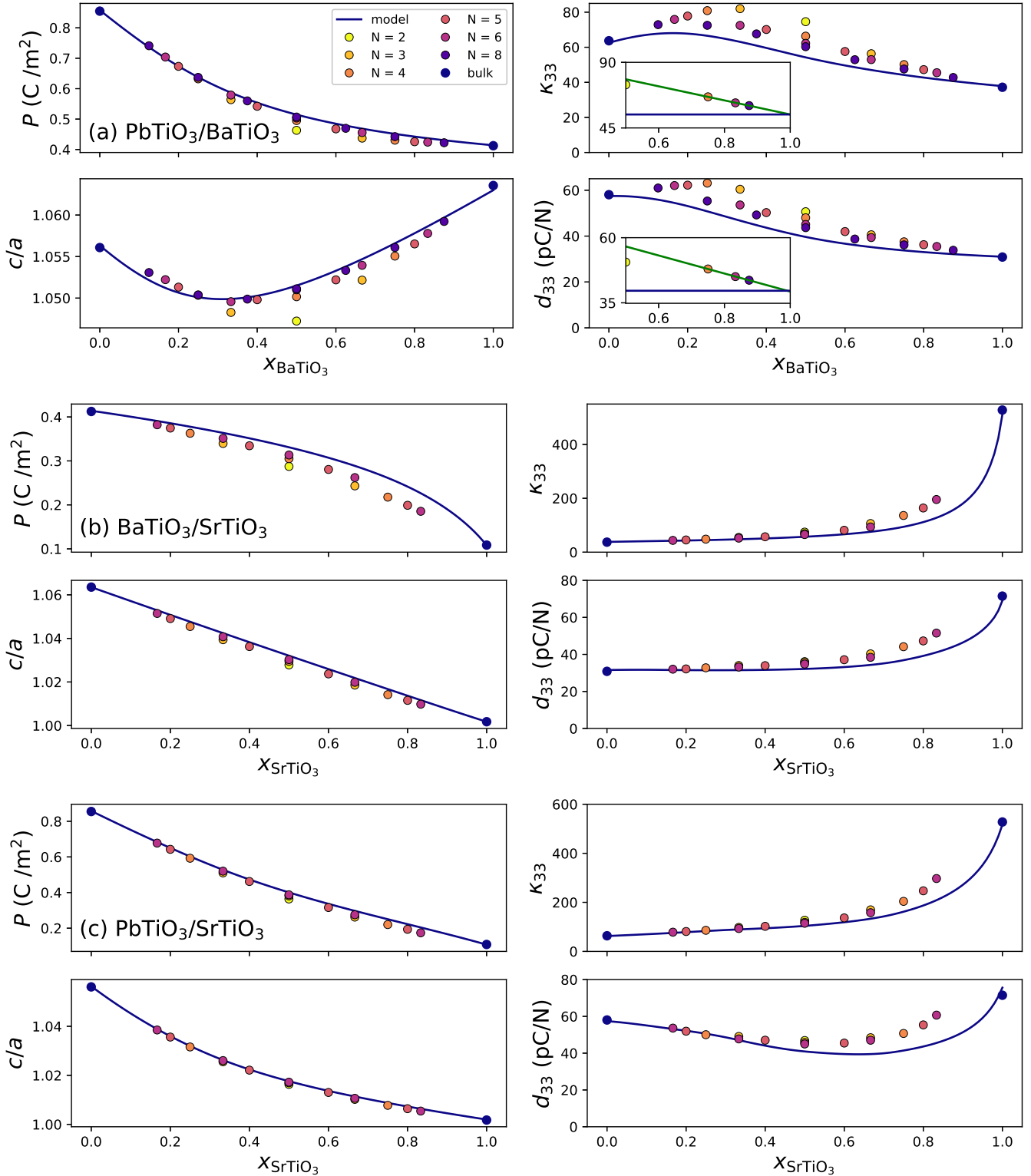[43] X. Wang and D. Vanderbilt, Physical Review B **75**, 115116 (2007).

FIG. 2: Spontaneous polarization, tetragonality (c/a), dielectric response κ_{33} and piezoelectric response d_{33} for (a) PbTiO$_3$/BaTiO$_3$, (b) BaTiO$_3$/SrTiO$_3$ and (c) PbTiO$_3$/SrTiO$_3$, plotted as functions of the layer fraction x of the lower polarization constituent. The bulk-layer model results are shown by a solid line and the first-principles results for individual superlattices are shown as circles filled by colors corresponding to the total superlattice period. The insets in the panels for κ_{33} and d_{33} of PbTiO$_3$/BaTiO$_3$ show the first-principles values for n:n superlattices ($x = 0.5$) plotted against $(1 - 1/N)$, where N is the superlattice period in layers of bulk unit cells, with a linear fit to the $N > 2$ values showing accurate convergence to the model value (indicated by the horizontal line). The differing scales of the vertical axes in each figure are chosen to accommodate the differing ranges over which properties vary between systems. The imperfect agreement between the end points and the model is discussed in the supplemental material [20].